Journal of Power Sources 247 (2014) 932–938

Contents lists available at ScienceDirect

Journal of Power Sources

journal homepage: www.elsevier.com/locate/jpowsour

Polymer electrolyte fuel cell performance of poly(arylene ether ketone)-graft-crosslinked-poly(sulfonated arylene ether sulfone)

Ryousuke Hara [a], Nobutaka Endo [a], Mitsuru Higa [a], Ken-ichi Okamoto [a, *], Xuan Zhang [b], Huiping Bi [b], Shanshan Chen [b], Zhaoxia Hu [b], Shouwen Chen [b]

[a] Graduate School of Science & Engineering, Yamaguchi University, Tokiwadai 2-16-1, Ube, Yamaguchi 755-8611, Japan
[b] School of Environmental & Biological Engineering, Nanjing University of Science & Technology, Nanjing 210094, China

HIGHLIGHTS

- Hydrophobic PAEK main chains were graft-crosslinked with hydrophilic SPAES segments.
- They were compared to sulfonated poly(arylene ether sulfone) multi-block copolymer.
- They showed much smaller water uptake and in-plane dimensional change.
- They showed much smaller hydrogen permeability.
- They showed higher or comparable PEFC performance and better PEFC durability.

GRAPHICAL ABSTRACT

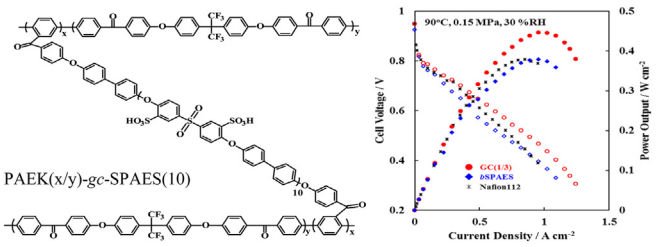

ARTICLE INFO

Article history:
Received 5 July 2013
Received in revised form
22 August 2013
Accepted 26 August 2013
Available online 18 September 2013

Keywords:
Sulfonated aromatic multiblock copolymer
Graft-crosslinked copolymer
Polymer electrolyte membrane
Polymer electrolyte fuel cell

ABSTRACT

The physical properties and polymer electrolyte fuel cell (PEFC) performance of the graft-crosslinked copolymers based on hydrophobic poly(arylene ether ketone) main chains graft-crosslinked with hydrophilic sulfonated poly(arylene ether sulfone) segments were investigated in comparison with those of the sulfonated poly(arylene ether sulfone) multi-block copolymer (*b*SPAES) and Nafion 112. The graft-crosslinked copolymers with ion exchange capacity (IEC) of 1.90 and 1.58 meq g^{-1} (GC(1/3) and GC(1/5), respectively) showed the much lower water uptakes and smaller *in-plane* dimensional changes than *b*SPAES with IEC of 2.04 meq g^{-1}, resulting in the higher membrane stability. GC(1/3) showed the highest PEFC performances at conditions of 90 °C, 0.2–0.1 MPa and 82–30% RH among these membranes. GC(1/5) also showed the higher or similar PEFC performances when compared to *b*SPAES and Nafion 112. GC(1/5) showed much better PEFC durability than *b*SPAES. The graft-crosslinked copolymers have high potential as polymer electrolyte membranes for fuel cell applications.

1. Introduction

Polymer electrolyte fuel cells (PEFCs) have been drawing great attention as energy sources for transportation, stationary and portable devices because of the environmentally friendly nature and the high fuel efficiency. Polymer electrolyte membrane (PEM) in a PEFC system plays a key role to transport protons from anode to cathode and to separate the fuel and oxidant. Sulfonated aromatic polymers have been extensively studied as alternative materials to the state-of-the-art perfluorosulfonic acid polymers [1–41]. However, most of these aromatic polymers showed low proton conductivity at low relative humidities. High performance PEMs are

* Corresponding author. Tel.: +81 836 85 9203; fax: +81 836 85 9601.
E-mail address: okamotok@yamaguchi-u.ac.jp (K.-i. Okamoto).

0378-7753/$ – see front matter © 2013 Elsevier B.V. All rights reserved.
http://dx.doi.org/10.1016/j.jpowsour.2013.08.121

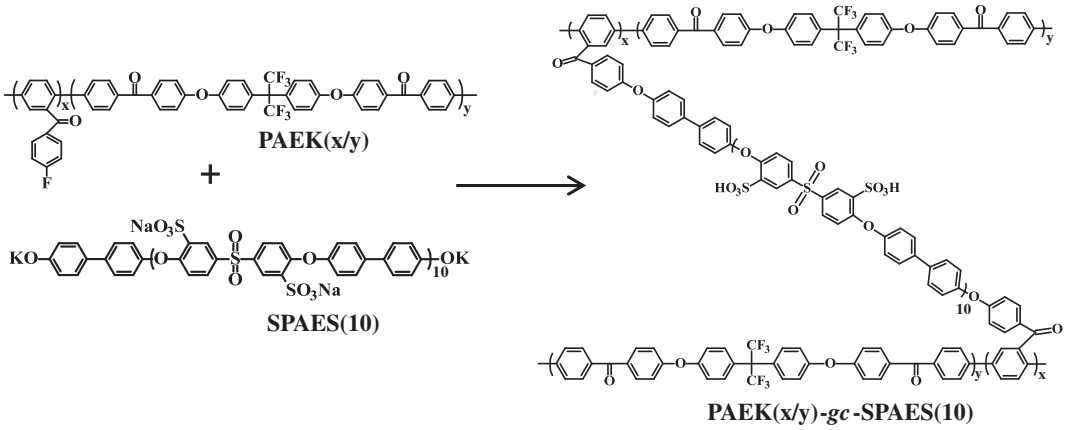

Fig. 1. Synthesis of graft-crosslinked copolymer PAEK(*x*/*y*)-*gc*-SPAES(10).

required to have high *through-plane* proton conductivity under the conditions of low relative humidity (<50 %RH) and high temperature (>80 °C). One of the effective strategies to overcome this drawback is to develop PEMs based on hydrophilic-hydrophobic multi-block [9,13–28] and graft (or comb-shaped) [29–33] copolymers having microphase-separated morphology suitable for PEFC applications.

Chen et al. developed the graft-crosslinked copolymer membranes based on hydrophobic poly(arylene ether ketone) main chains graft-crosslinked with hydrophilic sulfonated poly(arylene ether sulfone) segments, of which the chemical structure is shown in Fig. 1 [33]. The graft-crosslinked copolymer membranes exhibited the clear nano-scale phase-separated morphology and relatively high proton conductivity under 30–90% relative humidity (RH). In this study, the PEFC performances of the graft-crosslinked copolymer membranes have been investigated compared to those of the sulfonated poly(arylene ether sulfone) multi-block copolymer (*b*SPAES) and Nafion 112 membranes.

2. Experimental

2.1. Preparation of graft-crosslinked copolymer membranes

As illustrated in Fig. 1, the graft-crosslinked copolymer PAEK(*x*/*y*)-*gc*-SPAES(*l*) was prepared from poly[(4-fluorobenzoyl)phenylene-*co*-(arylene ether ketone)] (PAEK(x/y)) and sulfonated poly(-arylene ether sulfone) (SPAES(*l*), where x/y and *l* refer to the molar ratio and the block length, respectively, according to the reported method [33]. The membranes were prepared by casting the 5 wt% DMSO solution onto glass plates and dried at 80 °C for 2 h and then at 120 °C for 15 h, followed by residue extraction in acetone, proton exchange and curing.

2.2. Preparation of sulfonated poly(arylene ether sulfone) multi-block copolymer

The multi-block copolymer *b*SPAES, of which the hydrophilic and hydrophobic block length of 10, was prepared from the phenorate-end-capped hydrophilic oligomer and the fluorine-end-capped hydrophobic oligomer according to the reported method [23], as illustrated in Fig. 2. The membranes were prepared by the casting method as mentioned above.

The corresponding sulfonated poly(arylene ether sulfone) random copolymer (*r*SPAES) was also prepared from 3,3′-disulfo-4,4′-difluorodiphenyl sulfone, 4,4′-difluorodiphenyl sulfone and biphenol with a molar feed ratio of 6:4:10.

2.3. Membrane characterization

Mechanical tensile tests were performed on a universal testing machine (Orientic, TENSILON TRC-1150A) at 25 °C and around 50% RH. Ion exchange capacity (IEC) was determined by a titration method. A sample membrane in proton form was soaked in a 15 wt % NaCl solution at 40 °C for 72 h to exchange the H^+ ion with Na^+ ion. Released protons were titrated by a 0.02 N NaOH solution using phenolphthalein as an indicator.

Water uptake (WU) was measured by soaking a sample sheet in water at 30 °C for 24 h. Then the membrane was taken out, wiped with tissue paper very quickly, and weighed on a microbalance. Water uptake was calculated from eq. (1):

$$\mathrm{WU} = (W_s - W_d)/W_d \times 100\% \tag{1}$$

where W_d and W_s are the weights of dry and corresponding water-swollen membranes, respectively.

Dimensional changes in membrane thickness (Δt) and plane direction (Δl) were measured by soaking more than two sample sheets in water at 30 °C for 12 h. The measurement was performed using a dial gauge and a digital microscope (Keyence VH-5500) for thickness and length, respectively, in dry and wet states. The *through-plane* and *in-plane* dimensional changes and the anisotropic membrane swelling ratio ($\Delta_{t/l}$) were calculated from eq. (2):

$$\Delta t = (t - t_d)/t_d$$

$$\Delta l = (l - l_d)/l_d$$

$$\Delta_{t/l} = \Delta t/\Delta l \tag{2}$$

where t_d and l_d are the thickness and length of dry membrane, respectively; t and l refer to those of the membrane swollen in water.

In-plane and *through-plane* proton conductivity ($\sigma_{//}$and $\sigma_{\perp}$, respectively) was determined using an electrochemical impedance spectroscopy technique over the frequency from 10 Hz to 100 KHz (Hioki 3532-80). The resistance R associated with the membrane conductance was determined from a high-frequency intercept of the impedance with the real axis. For $\sigma_{//}$, a single cell with two platinum plate electrodes was mounted on a Teflon plate at 0.5 cm distance. The cell was placed under either in a thermo-controlled humidistat chamber or in liquid water. For $\sigma_{\perp}$, a membrane sample was set between two platinum plate electrodes of 1 cm^2 area, and mounted on two Teflon blocks [25]. The cell was placed in

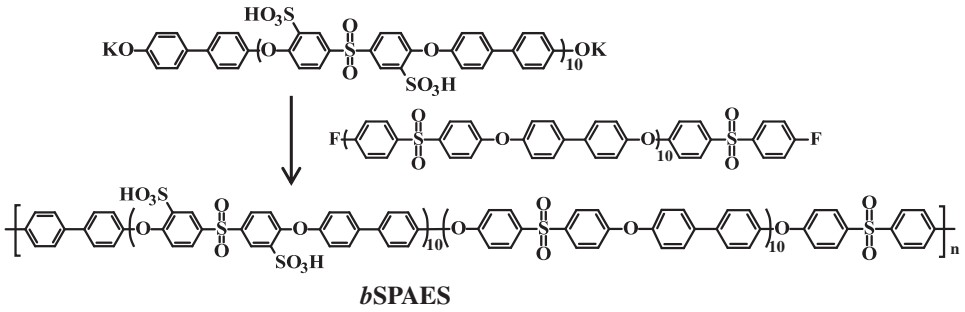

Fig. 2. Synthesis of sulfonated poly(arylene ether sulfone) multi-block copolymer *b*SPAES.

Table 1
Physical properties of the graft-crosslinked copolymer, sulfonated poly(arylene ether sulfone) block and random copolymer and Nafion 112 membranes.

Code	IEC[a]	*WU*[b]	λ[b]	Size change[b]		$\Delta_{t/l}$	$\sigma_{//}$[c]			$\sigma_{\perp}$[d]	$\sigma_{\perp}/\sigma_{//}$[d]
				Δt	Δl		50	70	Water	Water	
	(meq g^{-1})	(%)		(%)			(mS cm^{-1})				
GC(1/3)	1.90	66	19	20	11	1.8	19	52	231	184	0.80
GC(1/5)	1.58	44	16	15	8	2.0	12	39	186	140	0.75
*b*SPAES	2.04	91	25	34	14	2.4	17	61	230	210	0.91
*r*SPAES	2.35	123	29	34	27	1.3	11	43	261	245	0.94
Nafion 112	0.89	39	24	16	14	1.1	26	59	140	138	0.98

[a] By titration method.
[b] At 30 °C.
[c] under 50% RH and 70 %RH and in water at 60 °C.
[d] In water at 60 °C.

liquid water. Proton conductivity ($\sigma_{//}$and $\sigma_{\perp}$) was calculated from eq. (3):

$$\sigma_{\parallel} = d/(t_s w_s R)$$

$$\sigma_{\perp} = t_s/(AR) \quad (3)$$

where d is the distance between the two electrodes, t_s and w_s are the thickness and width of the membrane at a standard condition of 70% RH, respectively, A is the electrode area, and R is the resistance. The thickness of a water-swollen membrane was used in the calculation of both $\sigma_{//}$and $\sigma_{\perp}$ in the fully hydrated state. The *through-plane* conductivity measurement was performed only on the cell placed in water, because the contact resistance between electrodes and membrane could be neglected only in the fully hydrated state. The similar $\sigma_{\perp}$ values were obtained for the samples of single layer and double layers of membrane.

2.4. Fuel cell performance measurement

Catalyst electrodes were purchased from Johnson and Matthey Plc., #45372, of which the composition is as follows; non-woven carbon fibers: 75%; carbon black: 5%; polytetrafluoroethylene: 10%; catalyst (finely divided platinum metal on carbon): 5% and polyfluorosulfonic acid ionomers: 5%. The Pt loading was estimated to be 0.53 mg cm^{-2} from the thickness (0.022 mm) and weight of electrode. A MEA was fabricated from a membrane (5.0 cm × 5.0 cm) sample and the catalyst electrodes by hot-pressing an electrode/membrane/electrode sandwich at 130 °C for 5 min under 60 kg cm^{-2}. Prior to the hot-pressing, both surfaces (2.25 cm × 2.25 cm in area) of the membrane were coated with 0.05 cm^3 of 1.25 wt% Nafion/isopropanol solution to improve the adhesion between the membrane and the electrodes. The Nafion coated layers (0.5 μm in thickness) were reasonably considered not to affect the proton conduction and gas diffusion of PEM. The MEA was set in a single-cell test fixture (NF Inc., active area: 5 cm^2) and mounted in an in-house fuel cell station (NF Inc., model As-510), which was supplied with temperature-controlled humidified gases (H_2 and air). The PEFC performance was evaluated at a cell temperature of 90 °C, gas pressure of 0.2–0.1 MPa and gas humidifier temperatures of 85–61 °C. The gas flow was controlled to keep constant utilization of H_2 at 60, 70 or 80% and of air at 15, 30 or 50% depending on the humidification condition, although the lowest gas flow rate was limited at 20 Ncm^3 min^{-1}. The cell resistance (R_c) was determined by the AC impedance cole–cole plots. The *through-plane* proton conductivity under PEFC operation

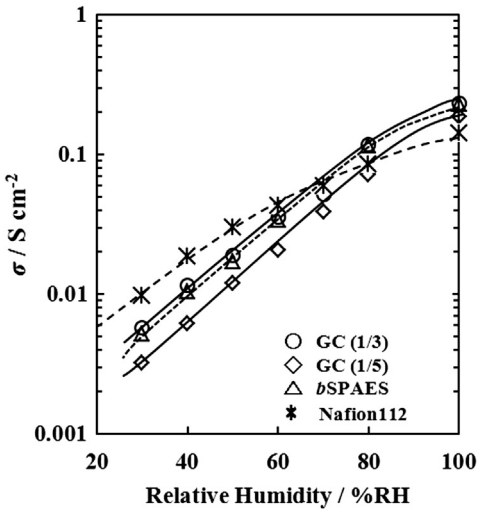

Fig. 3. Relative humidity dependence of *in-plane* conductivity for GC(1/3), GC(1/5), *b*SPAES and Nafion 112.

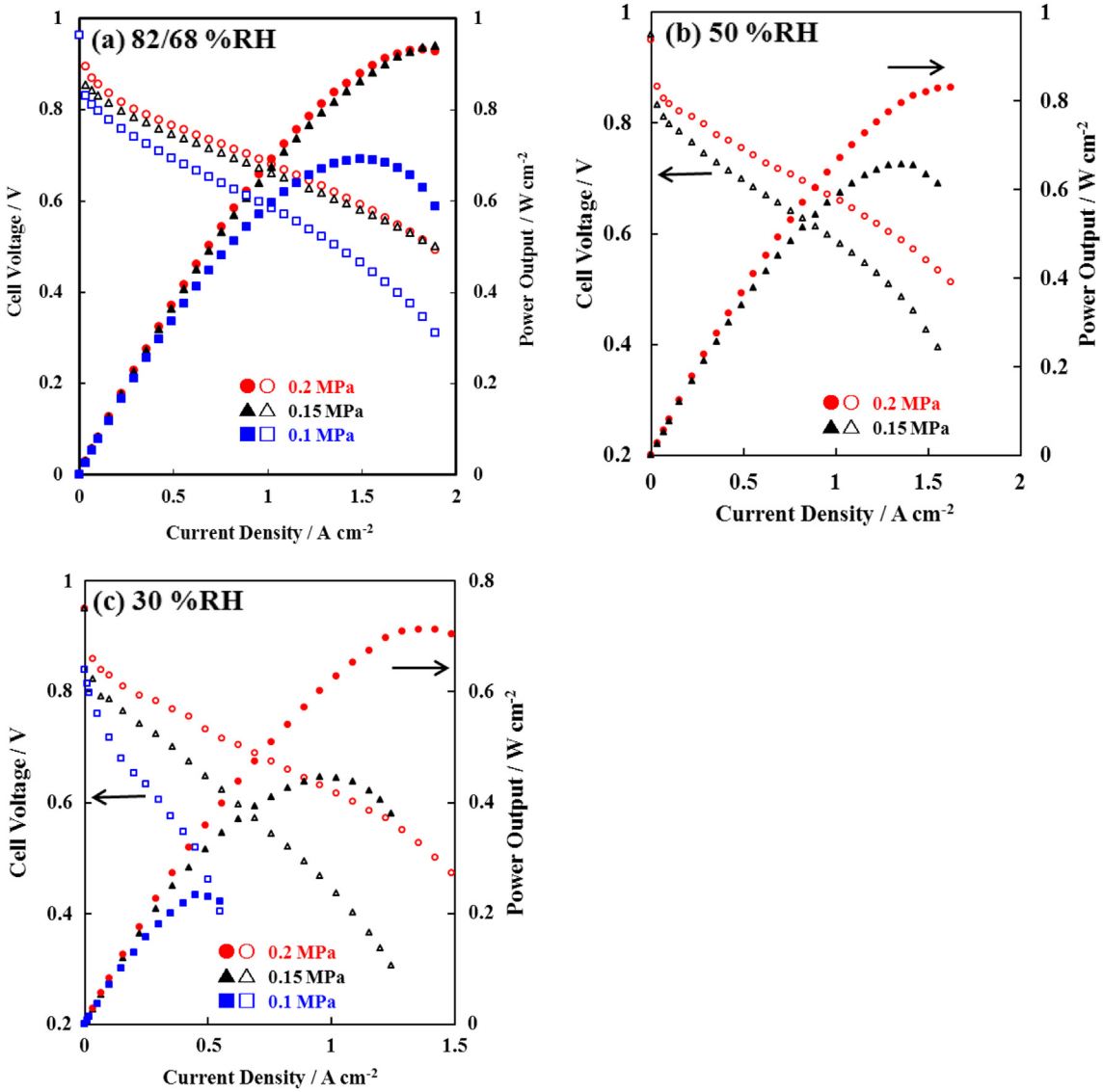

Fig. 4. Effect of feed gas pressure and humidification on PEFC performances for GC(1/3) at 90 °C.

($\sigma_{\perp,FC}$) was evaluated by assuming that the membrane resistance is approximately equal to the cell resistance.

3. Results and discussion

3.1. Physical properties

In this study, two types of the graft-crosslinked copolymer were used, that is, PAEK(1/3)-*gc*-SPAES(10) and PAEK(1/5)-*gc*-SPAES(10), which were abbreviated to GC(1/3) and GC(1/5), respectively. They were soluble in DMSO just after the graft-crosslinking reaction, but the membranes heat-treated at 120 °C for 15 h were insoluble. The sulfonated poly(arylene ether sulfone) multi-block copolymer *b*SPAES used for comparison had the same hydrophilic segment (block length: 10) as the hydrophilic graft segment for GC(1/3) and GC(1/5).

GC(1/3) and GC(1/5) exhibited similar and fairly high mechanical strength, that is, a Young's modulus of 1.0 GPa, a tensile stress at break of 34 MPa and an elongation at break of 27%. *b*SPAES exhibited a slightly lower Young's modulus of 0.80 GPa, a similar tensile stress at break and a higher elongation at break of 60%.

The physical properties of these membranes are listed in Table 1 together with the sulfonated poly(arylene ether sulfone) random copolymer (*r*SPAES) and Nafion 112 cited for comparison. The water uptake was in the order of *r*SPAES > *b*SPAES > GC(1/3) > GC(1/5) > Nafion 112. As the water uptake significantly depends on the IEC, the number of water molecules sorbed per sulfonic acid group (λ) was calculated using the IEC value determined by the titration method. The λ values for GC(1/3) and GC(1/5) (19 and 16, respectively) were much smaller than those for *b*SPAES, *r*SPAES and Nafion 112 (24–29).

GC(1/3) and GC(1/5) showed the slightly anisotropic membrane swelling in water, that is, the *through-plane* dimensional change (Δt) was about two times larger than the *in-plane* one (Δl). Although having the similar anisotropic swelling ratio of 2.4, *b*SPAES showed the much larger dimensional changes than GC(1/3) and GC(1/5). On the other hand, *r*SPAES and Nafion 112 showed the isotropic membrane swelling. As a result, the *in-plane* dimensional changes for GC(1/3) and GC(1/5) (11 and 8%, respectively) were

Table 2
PEFC performance data of GC(1/3), GC(1/5), *b*SPAES and Nafion 112 at 90 °C.

Conditions[a]	Code	OCV (V)	$V_{0.5}$ (V)	W_{max} (W cm^{-2})	$\sigma_{\perp,FC}$[b] (mS cm^{-1})
0.2/82[c]	GC(1/3)	1.00	0.75	0.93	95
	GC(1/5)	1.00	0.75	0.94	98
	*b*SPAES	1.02	0.74	>0.98	83
	Nafion 112	0.95	0.71	>0.90	93
0.15/82[c]	GC(1/3)	0.96	0.73	>0.94	92
	GC(1/5)	0.99	0.71	0.83	83
	*b*SPAES	1.00	0.71	>0.91	79
	Nafion 112	0.95	0.70	0.84	82
0.1/82[c]	GC(1/3)	0.96	0.69	0.69	73
	*b*SPAES	1.01	0.68	0.62	65
	Nafion 112	0.95	0.66	0.63	66
0.2/50	GC(1/3)	0.96	0.75	0.83	88
	GC(1/5)	1.01	0.71	0.78	78
	*b*SPAES	1.00	0.71	0.72	74
	Nafion 112	0.96	0.70	0.73	76
0.15/50	GC(1/3)	0.96	0.70	0.66	66
	GC(1/5)	1.01	0.67	0.64	59
	*b*SPAES	1.00	0.65	0.57	62
	Nafion 112	0.95	0.66	0.54	61
0.2/30	GC(1/3)	0.95	0.73	0.71	65
	GC(1/5)	1.02	0.68	0.63	62
	*b*SPAES	1.01	0.68	0.62	65
	Nafion 112	0.96	0.70	0.61	64
0.15/30	GC(1/3)	0.95	0.64	0.45	40
	GC(1/5)	1.02	0.58	0.34	(26)
	*b*SPAES	1.00	0.57	0.38	39
	Nafion 112	0.95	0.61	0.38	45
0.1/30	GC(1/3)	0.94	0.46	0.23	(15)

[a] PEFC operation conditions: x/y refer to gas pressure (MPa) and relative humidity (% RH).
[b] At 1 A cm^{-2}; the data in parentheses were measured at 0.5 A cm^{-2}.
[c] 82/68% RH.

much smaller than those of *b*SPAES, *r*SPAES and Nafion 112 (14, 27 and 14%, respectively). It is noted that the small *in-plane* dimensional changes for GC(1/3) and GC(1/5) lead to the high dimensional stability of their MEAs.

The *in-plane* proton conductivity ($\sigma_{//}$) at 60 °C as a function of relative humidity is summarized in Table 1 and Fig. 3. With decreasing the relative humidity, the $\sigma_{//}$decreased largely. GC(1/3), GC(1/5) and *b*SPAES showed the similar humidity dependence, which was larger than that for Nafion 112. Compared to GC(1/3) and *b*SPAES, GC(1/5) had the smaller $\sigma_{//}$values in whole humidity range because of the smaller IEC of 1.58 meq g^{-1}. The conductivity of GC(1/3) with the IEC of 1.90 meq g^{-1} was comparable to that of *b*SPAES with the slightly larger IEC of 2.04 meq g^{-1} in whole humidity. *r*SPAES showed the much lower conductivity than GC(1/3) and *b*SPAES in the low relative humidity range in spite of higher IEC of 2.35 meq g^{-1}. This is because GC(1/3), GC(1/5) and *b*SPAES have the micro-phase separated morphology, whereas *r*SPAES has the homogeneous morphology [13–21,33].

The *through-plane* and *in-plane* proton conductivity ($\sigma_{\perp}$ and $\sigma_{//}$, respectively) and the anisotropic proton conductivity ratio ($\sigma_{\perp}/\sigma_{//}$) in water at 60 °C are summarized in Table 1 *r*SPAES and Nafion 112 showed the isotropic proton conductivity ($\sigma_{\perp}/\sigma_{//}$ = 0.94–0.98). *b*SPAES also showed the almost isotropic conductivity ($\sigma_{\perp}/\sigma_{//}$ = 0.91) in spite of the slightly anisotropic membrane swelling behaviour ($\Delta_{t/l}$ = 2.4). On the other hand, GC(1/3) and GC(1/5) showed the slightly anisotropic proton conductivity ($\sigma_{\perp}/\sigma_{//}$ = 0.80–0.75).

3.2. Fuel cell performance

Fig. 4(a)–(c) shows the effects of feed gas pressure and humidification on PEFC performance for GC(1/3) (49 μm in thickness) at a cell temperature of 90 °C. Anode/cathode gas humidification temperatures were set at 85/80, 72.8/72.8 and 61.3/61.3 °C, which correspond to 82/68%, 50% and 30% RH, respectively. Table 2 lists the PEFC performance data of open circuit voltage (OCV), cell voltage at a current density of 0.5 A cm^{-2} ($V_{0.5}$), maximum output (W_{max}) and *through-plane* proton conductivity ($\sigma_{\perp,FC}$) under PEFC operation. In general, the $\sigma_{\perp,FC}$ value is larger than the $\sigma_{//}$value especially for the lower humidification due to the additional humidification caused by the back-diffusion of water formed at the cathode [37–39]. The back-diffusion of water is less effective for the membrane with a lower IEC and at a lower feed gas pressure.

At the relatively high humidification of 82/68% RH, the PEFC performance hardly decreased with a decrease in gas pressure from 0.2 MPa to 0.15 MPa, but fairly decreased with a decrease to 0.1 MPa (ambient pressure), that is, $V_{0.5}$ decreased from 0.75 V to 0.69 V and W_{max} decreased from 0.93 W cm^{-2} to 0.69 W cm^{-2}. At 0.2 MPa, the PEFC performance slightly decreased with a decrease in gas humidification from 82/68% RH to 50% RH, but fairly decreased with a decrease to 30% RH. However, the PEFC performance at 30% RH was still kept in a reasonably high level ($V_{0.5}$: 0.73 V and W_{max}: 0.71 W cm^{-2}). A decrease in gas pressure at the lower gas humidification caused a larger reduction in the cell performance. At 30% RH, the cell performance at 0.15 MPa (0.64 V and 0.45 W cm^{-2}) was much lower when compared to 0.2 MPa. In these cases, the $\sigma_{\perp,FC}$ values reflected the PEFC performances. The high PEFC performances were observed at the conditions of 0.2–0.15 MPa/82%RH and 0.2 MPa/50% RH, where the $\sigma_{\perp,FC}$ values were 95–88 mS cm^{-1}. The middle PEFC performances were observed at 0.1 MPa/82%RH, 0.15 MPa/50% RH and 0.2 MPa/30%RH, where the $\sigma_{\perp,FC}$ values were 73–65 mS cm^{-1}. The low PEFC performances were observed at 0.15–0.1 MPa/30%RH, where the $\sigma_{\perp,FC}$ values were 40–15 mS cm^{-1}.

For comparison, the PEFC performance data of GC(1/5) (57 μm), *b*SPAES (35 μm) and Nafion 112 (55 μm) are also listed in Table 2. Fig. 5 shows comparison of PEFC performances at 90 °C, 0.15 MPa and different humidification of 82/68% RH, 50% RH and 30% RH. In general, the thinner membrane tends to give the higher PEFC performance because of the lower membrane resistance and more effective back-diffusion of water, unless the hydrogen crossover becomes too large. At 82/68% RH and 0.2–0.15 MPa, every membrane showed the high PEFC performance. For example, at 82/68% RH and 0.15 MPa, GC(1/3) showed the high performance of $V_{0.5}$: 0.73 V and W_{max}: >0.94 W cm^{-2}, which was similar to that of *b*SPAES, and slightly higher than those of GC(1/5) and Nafion 112. At the other conditions, GC(1/3) showed the highest PEFC performances among these membranes. For example, at 50% RH and 0.15 MPa, GC(1/3) showed the reasonably high PEFC performance (0.70 V and 0.66 W cm^{-2}), which was fairly higher than that of *b*SPAES (0.65 V and 0.57 W cm^{-2}). GC(1/5) also showed the higher or similar PEFC performances except for 30% RH and 0.15 MPa when compared to *b*SPAES and Nafion 112. These results indicate that GC(1/3) and GC(1/5) have much higher potential as PEM under the lower humidification than *b*SPAES, taking their larger membrane thicknesses and lower IECs into account. This may be due to difference in the membrane morphology. The micro-phase separated structure may be better-developed for GC(1/3) and GC(1/5) membranes than for *b*SPAES membrane because the hydrophobicity of the hydrophobic segment is higher for PAEK(*x*/*y*) than for oligo(arylene ether sulfone).

Hydrogen permeability coefficient (P_{H_2}) was calculated from hydrogen crossover current at 90 °C, 88% RH and 0.2 MPa. The P_{H2} values were 20, 24, 90 and 113 Barrer (1 Barrer = 1 × 10^{-10} cm^3(STP) cm cm^{-2} s^{-1} cm Hg^{-1}) for GC(1/3), GC(1/5), *b*SPAES and Nafion 112, respectively. The P_{H2} values for GC(1/3) and (1/5) were much smaller than those for *b*SPAES and Nafion 112.

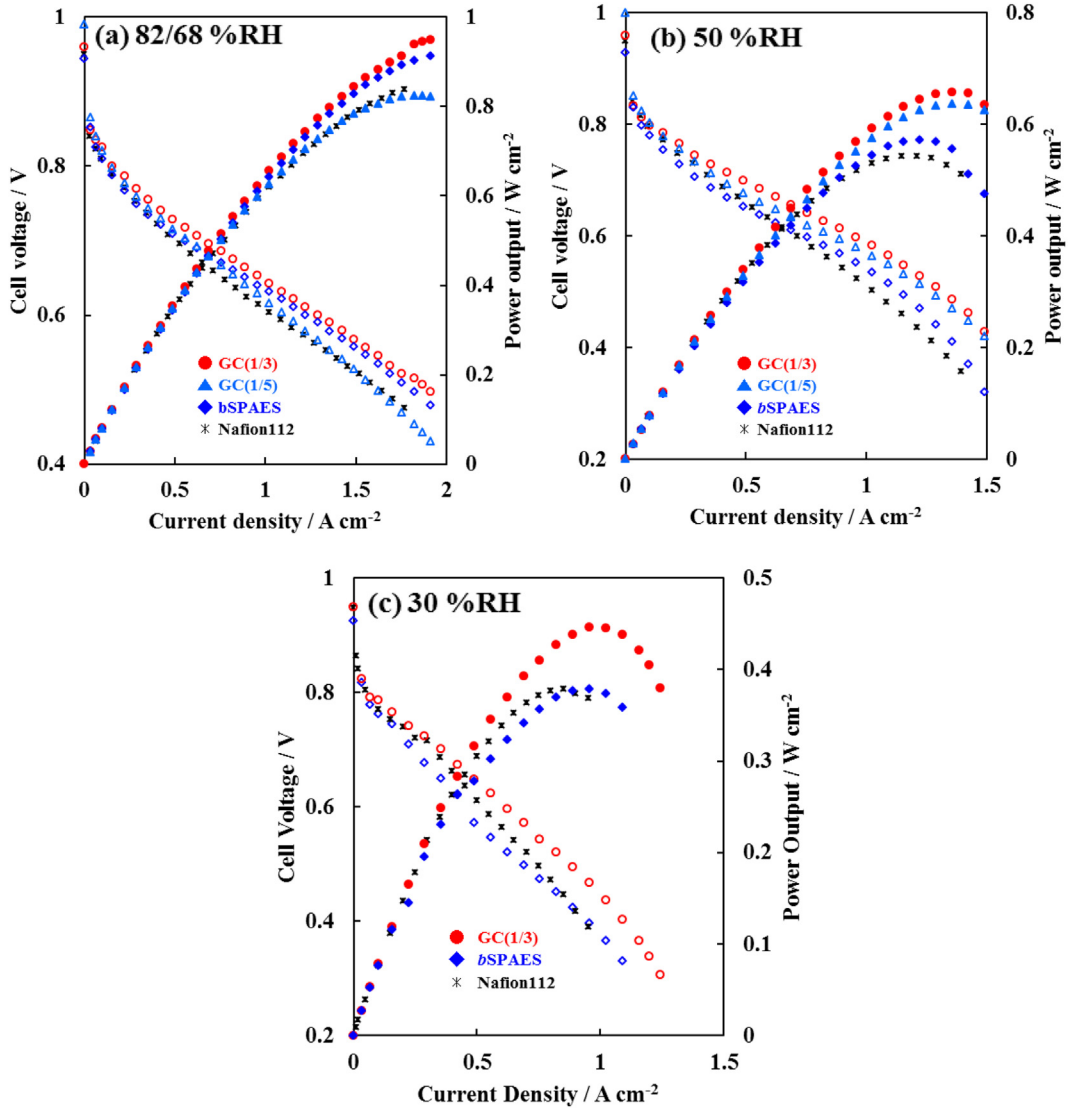

Fig. 5. PEFC performances of GC(1/3), GC(1/5), *b*SPAES and Nafion 112 at 90 °C, 0.15 MPa and (a) 82/68% RH, (b) 50% RH and (c) 30% RH.

For the durability test, PEFC cells with *b*SPAES and GC(1/5) were operated at 90 °C, 0.2 MPa and 50% RH under a constant load current density of 0.2 or 0.5 A cm^{-2} with monitoring the cell voltage and cell resistance. The results are shown in Figs. 6 and 7. In the case of *b*SPAES, as shown in Fig. 6, the cell voltage and OCV were held with the small decreases for 390 h. However, after 390 h, the cell voltage and OCV suddenly dropped and the operation was stopped, indicating some fatal damage of membrane. The PEFC

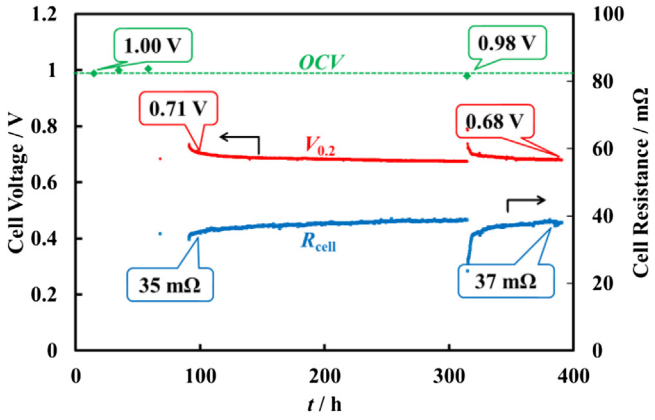

Fig. 6. Durability test of PEFC with *b*SPAES at 90 °C, 0.15 MPa, 50% RH and 0.2 A cm^{-2}.

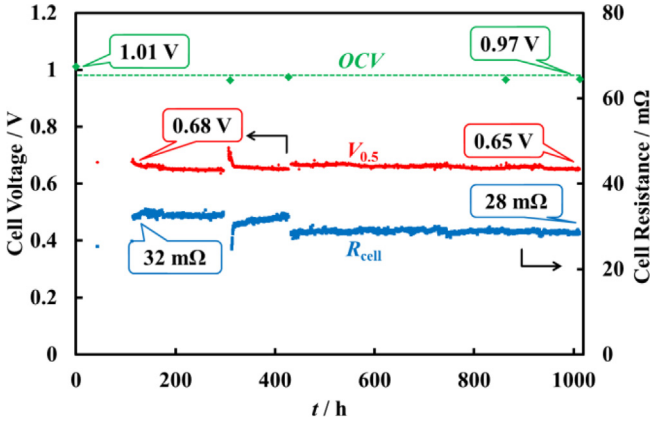

Fig. 7. Durability test of PEFC with GC(1/5) at 90 °C, 0.15 MPa, 50% RH and 0.5 A cm^{-2}.

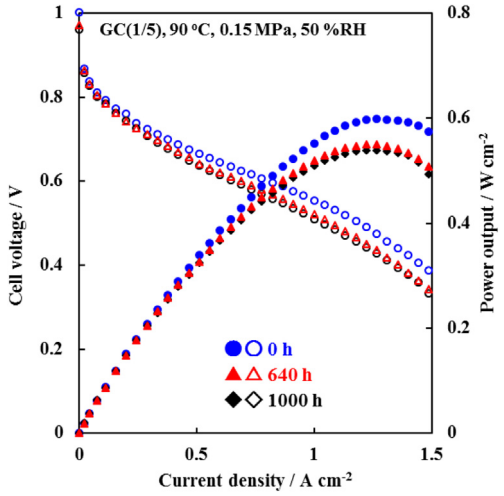

Fig. 8. PEFC performances of GC(1/5) at 90 °C, 0.15 MPa and 50% RH before and after the durability test.

durability of *b*SPAES was rather poor. In the case of GC(1/5), as shown in Fig. 7, the cell voltage and OCV were held with only the small decreases (0.03–0.04 V) for 1000 h. The polarization and power output curves were measured at 90 °C, 0.15 MPa and 50% RH after 640 h and 1000 h and compared to those before the durability test. The results are shown in Fig. 8. The relatively small reduction in the PEFC performance occurred by 640 h, but no further reduction was observed after 1000 h. It is noted that PAEK-*gc*-SPAES membranes had much higher PEFC durability than *b*SPAES membranes. Both types of membranes had the same hydrophilic segment (SPAES with a block length of 10) but showed the different water sorption behaviour. The former membranes showed the lower water uptake and the smaller *in-plane* dimensional change, which might reduce the radical attack in the hydrophilic domains and the stress between the membrane and the electrodes.

4. Conclusions

The graft-crosslinked copolymers with IECs of 1.90 and 1.58 meq g^{-1} (GC(1/3) and GC(1/5), respectively) showed the much lower water uptakes and smaller *in-plane* dimensional changes than *b*SPAES with an IEC of 2.04 meq g^{-1}. GC(1/3) showed the highest PEFC performances at conditions of 90 °C, 0.2–0.1 MPa and 82-30% RH among these membranes. GC(1/5) also showed the higher or similar PEFC performances when compared to *b*SPAES and Nafion 112. GC(1/5) showed much better PEFC durability than *b*SPAES. The graft-crosslinked copolymers have high potential as polymer electrolyte membranes for fuel cell applications.

Acknowledgements

The work conducted at Nanjing University of Science & Technology was partially supported by the National Natural Science Foundation of China (21006052, 21276128) and the Fundamental Research Funds for the Central Universities (30920130121014).

References

[1] O.J. Savadogo, New Mater. Electrochem. Syst. 1 (1998) 47–66.
[2] M. Rikukawa, K. .Sanui, Prog. Polym. Sci. 5 (2000) 1463–1502.
[3] J. Kerres, J. Membr. Sci. 185 (2001) 3–27.
[4] K.D. Kreuer, J. Membr. Sci. 185 (2001) 29–39.
[5] M. Hickner, H. Ghassemi, Y. Kim, B. Einsla, J.E. McGrath, Chem. Rev. 104 (2004) 4587–4661.
[6] W.L. Harrison, M.A. Hicker, Y.S. Kim, J.E. McGrath, Fuel Cells 5 (2005) 201–212.
[7] Y. Yin, O. Yamada, K. Tanaka, K. .Okamoto, Polym. J. 38 (2006) 197–219.
[8] C. Marestin, G. Gebel, O. Diat, R. Mercier, Adv. Polym. Sci. 216 (2008) 185–258.
[9] K. Goto, I. Rozhabskii, Y. Yamakawa, T. Otsuki, Y. Naito, Polym. J. 41 (2009) 95–105.
[10] T.J. Peckham, S. Holdcroft, Adv. Mater. 22 (2010) 4667–4690.
[11] M.A. Hickner, Mater. Today 13 (2010) 34–41.
[12] H. Zhang, P.K. Shen, Chem. Rev. 112 (2012) 2780–2832.
[13] H. Ghassemi, J.E. McGrath, T.A. Zawodzinski, Polymer 47 (2006) 4132–4139.
[14] Y.S. Kim, B. Einsla, M. Sankir, W. Harrison, B.S. Pivovar, Polymer 47 (2006) 4026–4035.
[15] M.L. Einsla, Y.S. Kim, M. Hawley, H.S. Lee, J.E. McGrath, B. Liu, M.D. Guiver, B.S. Pivovar, Chem. Mater. 20 (2008) 5636–5642.
[16] H. Lee, A. Roy, O. Lane, M. Lee, J.E. McGrath, J. Polym. Sci. Part A Polym. Chem. 48 (2010) 214–222.
[17] Y. Chen, C.H. Lee, J.R. Rowlett, J.E. McGrath, Polymer 53 (2012) 3143–3153.
[18] B. Bae, T. Yoda, K. Miyatake, K. Uchida, M. Watanabe, Angew. Chem. Int. Ed. 49 (2010) 317–320.
[19] F. Schonberger, J.A. Kerres, J. Polym. Sci. Part A Polym. Chem. 45 (2007) 5237–5255.
[20] K. Nakabayashi, K. Matsumoto, T. Higashimura, M. Ueda, J. Polym. Sci. Part A Polym. Chem. 46 (2008) 7332–7341.
[21] K. Nakabayashi, T. Higashihara, M. Ueda, J. Polym. Sci. Part A Polym. Chem. 48 (2010) 2757–2764.
[22] S. Takamuku, P. Jannasch, Adv. Energy Mater. 2 (2012) 129–140.
[23] X. Zhang, Z. Hu, S. Zhang, S. Chen, S. Chen, J. Liu, L. Wang, J. Appl. Polym. Sci. 121 (2011) 1707–1716.
[24] H. Bi, H. Chen, X. Chen, K. Chen, N. Endo, M. Higa, K. Okamoto, L. Wang, Macromol. Rapid Commun. 30 (2009) 1852–1856.
[25] Z. Hu, Y. Yin, K. Yaguchi, N. Endo, M. Higa, K. Okamoto, Polymer 50 (2009) 2933–2943.
[26] K. Chen, Z. Hu, N. Endo, M. Higa, K. Okamoto, Polymer 52 (2011) 2255–2262.
[27] S. Chen, K. Chen, X. Zhang, R. Hara, N. Endo, M. Higa, K. Okamoto, L. Wang, Polymer 54 (2013) 236–245.
[28] S. Chen, K. Chen, X. Zhang, N. Endo, M. Higa, K. Okamoto, L. Wang, J. Mater. Chem. A (2013), http://dx.doi.org/10.1039/C3TA11190CJ.
[29] E.M.W. Tsang, Z. Zhang, Z. Shi, T. Soboleva, S. Holdcroft, J. Am. Chem. Soc. 129 (2007) 15106–15107.
[30] D.S. Kim, Y.S. Kim, M.D. Guiver, J. Ding, B.S. Pivovar, J. Power Sources 182 (2008) 100–105.
[31] K. Yamazaki, H. Kawakami, Macromolecules 43 (2010) 7185–7191.
[32] N. Li, C. Wang, S.Y. Lee, C.H. Park, Y.M. Lee, M.D. Guiver, Angew. Chem. 123 (2011) 9324–9327.
[33] X. Zhang, Z. Hu, L. Luo, S. Chen, J. Liu, S. Chen, L. Wang, Macromol. Rapid Commun. 32 (2011) 1108–1113.
[34] N. Asano, M. Aoki, S. Suzuki, K. Miyatake, H. Uchida, M. Watanabe, J. Am. Chem. Soc. 128 (2006) 1762–1770.
[35] A. Kabasawa, J. Saito, H. Yano, K. Miyatake, H. Uchida, M. Watanabe, Electrochim. Acta 54 (2009) 1076–1782.
[36] Y. Yin, O. Yamada, S. Hayashi, K. Tanaka, H. Kita, K. Okamoto, J. Polym. Chem. Part A Polym. Chem. 44 (2006) 3751–3762.
[37] N. Endo, K. Matsuda, K. Yaguchi, Z. Hu, K. Chen, M. Higa, K. Okamoto, J. Electrochem. Soc. 156 (2009) B628–B633.
[38] K. Yaguchi, K. Chen, N. Endo, M. Higa, K. Okamoto, J. Power Sources 195 (2010) 4676–4684.
[39] K. Okamoto, K. Yaguchi, H. Yamamoto, K. Chen, N. Endo, M. Higa, H. Kita, J. Power Sources 195 (2010) 5856–5861.
[40] K. Yoshimura, K. Iwasaki, Macromolecules 42 (2009) 9302–9306.
[41] R.J. Stanis, M.A. Yaklin, C.J. Cornelius, T. Takatera, A. Umemoto, A. Ambrosini, C.H. Fujimoto, J. Power Sources 195 (2010) 104–110.